Journal of Materials Chemistry C

ARTICLE

High-Performance Ultralow Dielectric Constant Carbon-bridged Mesoporous Organosilica Films for Advanced Interconnects

Tao Jiang,[a] Bao Zhu,[a] Shi-Jin Ding,[a*] Zhongyong Fan,[b] and David Wei Zhang[a]

Mesoporous organosilica (MO) films are prepared using precursor 1,2-bis(triethoxysilyl)ethane (BTEE) and porogen template poly(ethylene oxide)–poly(propylene oxide)–poly(ethylene oxide) (P123). The effects of annealing temperature, P123/BTEE molar ratio, and moisture adsorption on the characteristics of the MO films are investigated. It is indicated that MO films prepared at a P123/BTEE molar ratio of 0.016 display the lowest dielectric constant (κ) of 1.80, a small dissipation factor of 0.0068 at 100 kHz, an extremely low leakage current density of 2.01×10^{-9} A cm^{-2} at 0.5 MV cm^{-1}, a modulus (E) of 6.27 GPa, and hardness (H) of 0.58 GPa. Following moisture adsorption, κ value increases by ~12%. However, ultraviolet treatment significantly reduces the extent of increase of the κ value to 4%. The films maintain an ultralow κ value of ~2.0 and a very low leakage current density of 1.7×10^{-9} A cm^{-2} at 0.5 MV cm^{-1}. Following annealing at 500 °C, the superior performance of the MO films is demonstrated by their κ value of ~1.92, leakage current density of 7.08×10^{-9} at 0.5 MV cm^{-1}, and improved E of ~9.1 GPa and H of ~0.8 GPa. Such MO films are very promising for advanced interlevel insulators.

Introduction

As the average feature size in ultra-large-scale integrated-circuits (ICs) continues to decrease according to Moore's Law, reducing the dielectric constant (κ) of interlevel dielectrics (ILDs) becomes more and more stringent to minimize parasitic resistance–capacitance (RC) delay, power consumption, and cross-talk noise.[1] According to the International Technology Roadmap for Semiconductors (ITRS 2012), ILDs with a bulk κ of 1.8–2.2 are required beyond 2021.[2] On the other hand, to achieve global and local wafer planarity, the chemical-mechanical-planarization (CMP) process is extensively used in the semiconductor industry. Therefore, the mechanical properties of ILDs, such as Young's modulus and hardness, are of critical importance to achieving a reliable CMP process. In particular, Young's modulus values greater than 4 GPa are required for the application of low-κ materials in the semiconductor industry.[3] Moreover, low-κ materials featuring excellent thermal stability and humidity resistance are highly desirable for practical application; otherwise, the reliability and lifetime of the chip will be reduced.

To achieve ultralow-κ ILDs, the incorporation of low-polarizable chemical bonds and free pores is considered to be a smart strategy. As one of the most promising ultralow-κ candidates, mesoporous organosilica (MO) films have been intensively studied as the next-generation interlevel dielectrics.[4-7] MO films are a unique class of inorganic–organic hybrid materials that contain organic groups as an integral part of the framework structure.[8] This is attributed to the incorporation of free nanopores ($\kappa = 1$) and low-polarizable bonds such as Si–C, C–C, and C–H. In principle, MO films can be prepared by cooperative assembly of network-forming precursors and structure-directing organic templates such as surfactants or block copolymers. These porogen templates can be decomposed upon thermal treatment at a specific temperature, consequently generating voids within the framework. This therefore leads to the formation of ultralow-κ films.

To date, various methods have been reported to prepare MO films such as sol–gel processes via spin-coating and dip-coating,[9,10] hydrothermal processes at the liquid–air and the solid–liquid interfaces,[11,12] selective mineralization of preorganized organic templates in supercritical carbon dioxide,[13,14] and vacuum-assisted aerosol deposition.[6] However, owing to the versatility of the sol–gel chemistry process, thermally sensitive bonds, organic molecules and polymers can be introduced either at the pore surfaces or within the network, thereby enabling control of the pore size, distribution, and organization.[3] Moreover, solution-based low-κ materials have certain advantages such as easy processing, flexibility with regard to chemical species, and control over the structure of the thin films through molecular design.[15] On the other hand, although plasma-enhanced chemical vapor deposition (PECVD) has been extensively employed to grow low-κ SiCOH (elementally descriptive and not representing the stoichiometry) films from various organosiloxanes and organosilane-based precursors, which exhibit various κ values between 2.4 and 3,[16-18] it is very challenging to achieve ultralow κ dielectrics of $\kappa < 2.4$. This is because PECVD is a high-energy process that can destroy organic moieties via unwanted side reactions.[19] Thus, it is non-feasible to retain these organic functionalities featuring low κ values in the fabrication of such PECVD films. Thus, the spin-coating deposition is the preferred method to preparing ultralow-κ films. Spin-coating deposition displays great potential because of its excellent gap filling, good planarization, and low cost of ownership.[20]

In this work, precursor 1,2-bis(triethoxysilyl)ethane (BTEE) was

This journal is © The Royal Society of Chemistry 2013

J. Mater. Chem. C, 2014, **XX**, XX | 1

selected and poly(ethylene oxide)–poly(propylene oxide)–poly(ethylene oxide) (P123) was used as a porogen. Compared with multi-precursors, the utilization of unique precursor in this article ensures easy control of preparation process and good uniformity of film composition over a large area. Furthermore, it is worth mentioning that CH_2–CH_2 is present between silicon atoms in the precursor monomer structure, enabling facile incorporation of carbon bridging units in the organosilicate network after hydrolyzation and condensation reactions between the BTEE monomers. Carbon bridging units are suitable for achieving excellent mechanical properties at high levels of porosity.[3] Furthermore, by optimizing the P123/BTEE molar ratio, ultralow-κ MO films with relatively good thermal stability and mechanical properties are achieved; the improved humidity resistance is also demonstrated following ultraviolet treatment.

Experimental

Synthesis

BTEE (96%, Gelest) and P123 (Aldrich) were used without further purification and all the reagents were purchased. Synthesis of the MO films first involved mixing deionized water with HCl (3.33×10^{-3} M, analytically pure, China) and anhydrous ethanol (99.7 wt.%, China). P123 was then dissolved in the above-prepared solution. Following homogeneous mixing, BTEE was added. The molar ratios of each component are shown in Table 1. The P123/BTEE molar ratio was varied to control the film structure and monitor the resulting film performance. In a typical MO film synthesis, BTEE (1.77 g, 5×10^{-3} M), P123 (0.575 g, 0.8×10^{-4} M), HCl (54 μL, 1.8×10^{-4} M), deionized water (3.6 g, 0.2 M), and ethanol (6.394 g, 0.139 M) were mixed until a homogeneous and clear solution was achieved. The optimum stirring time and temperature were 2 h and 60 °C, respectively. The films were spin-coated on low-resistivity silicon wafers (0.005–0.008 Ω cm) with a rotating speed of 3500–4000 rpm, and then cured in an oven at 60 °C for 65 h.

Table 1 Molar ratios of components used for film synthesis.

BTEE	P123 ($\times 10^{-3}$)	HCl ($\times 10^{-3}$)	H_2O	Ethanol
0.5	6	18	20	13.9
0.5	7	18	20	13.9
0.5	8	18	20	13.9
0.5	9	18	20	13.9
0.5	10	18	20	13.9
0.5	12	18	20	13.9

To evaluate the decomposition temperature of P123 in the as-coated films, the film prepared with a typical P123/BTEE molar ratio was calcined from 120 to 500 °C. After that, the films prepared with different P123/BTEE molar ratios were annealed at 350 °C, which was considered as the optimum annealing temperature, for 1 h in a flowing nitrogen atmosphere at a heating rate of 5 °C min^{-1}. Also, the representative MO films were annealed at 420 and 500 °C for 30 min in N_2 to evaluate the thermal stability of the prepared films.

To obtain the κ value of the resulting film, metal–insulator–semiconductor (MIS) capacitors were fabricated, and circular Al electrodes of 450 and 500 μm in diameter were prepared by a shadow mask using an electron beam evaporator.

Post-treatment of the Synthesized Films

To improve the moisture adsorption characteristics of the synthesized MO films, the ultralow-κ sample was exposed to ultraviolet (UV) irradiation at wavelengths of 200–400 nm for 5 h. During the UV irradiation process, the above-mentioned sample was stored in an ambient atmosphere at a constant temperature of 40–50 °C. To assess the moisture adsorption characteristics of the ultralow-κ films, various samples were kept in a box at 80% relative humidity (RH) under atmospheric pressure and room temperature for 15 h.

Characterization

Fourier transform infrared (FTIR) spectroscopy measurements were carried out on a spectrometer (Thermo Fisher, Nicolet 6700) in the mid-infrared region (4000–400 cm^{-1}). The surface and cross-section morphologies of the MO films were observed using atomic force microscopy (AFM, VEECO Multimode 8, USA) and transmission electron microscopy (TEM, FEI TECNAI G2 F20 S-TWIN), respectively. The film thickness and refractive index were measured on an ellipsometer (SOPRA GES 5E, France) and the thickness was confirmed by TEM measurements. The mechanical properties of the films were determined by an in situ nanomechanical test system with a Berkovid tip (TI-700 Ubi, Hysitron, Inc., USA). The dynamic continuous function was used to measure load–displacement curves, and the indentation displacement for each film was unified at 50 nm (~1/10 of the thickness of the measured films). Nitrogen adsorption–desorption isotherms were measured on a Micromeritics Tristars 3000 analyzer at 77 K. Before the measurements, the samples were outgassed at 200 °C in vacuum for 6 h. The pore-size distributions were derived from the adsorption branches of the isotherms using the Barrett–Joyner–Halanda (BJH) method. The elemental composition of the film was characterized by X-ray photoelectron spectroscopy (XPS) (Kratos Axis Ultra DLD).

The κ value of the film was calculated according to the equation $\kappa = Cd/\varepsilon_0 A$, where C is the capacitance of the MIS capacitor at 100 kHz, d is the thickness of the film, A is the area of the top electrode, and ε_0 is the permittivity of vacuum. Capacitance–voltage (C–V) characteristics were measured on a precision impedance analyzer (4294A, Agilent Technologies, Malaysia) with a 200-mV AC amplitude, and current–voltage (I–V) measurements were performed on a semiconductor device analyzer (B1500A, Agilent Technologies, Japan).

Results and discussion

To obtain the MO films, the porogen molecules (i.e., P123) that were initially incorporated in the spin-coated organosilica films need to be removed effectively. Therefore, the effect of annealing temperature on the removal of P123 was first investigated. Figure 1 shows the FTIR spectra of the spin-coated films as a function of post-annealing temperature. The as-prepared film displays a broad absorption band between 960 and 1200 cm^{-1} that corresponds to C–O stretching modes of P123 and Si–O bonds of BTEE, of which the absorption bands are concentrated at ~1080 cm^{-1} and ~1030 cm^{-1},[21-23] respectively. The absorption peaks centered at 2972 cm^{-1} and ~2887 cm^{-1} are attributed to C–H stretch vibrations of the CH_3 groups and methylene bridges, respectively.[7] The broad absorption band near 3365 cm^{-1} corresponds to hydroxyl groups vibrations, and the distinct absorption peak at 910 cm^{-1} is ascribed to Si–OH groups.[23] When the annealing temperature increases to 220 °C, the strong peak that is originally observed at ~1100 cm^{-1} becomes a shoulder. This indicates that thermal treatment can effectively remove the porogen P123. Furthermore, both the peak at 910 cm^{-1} and the band at ~3365 cm^{-1} almost disappear, indicating the

2 | *J. Mater. Chem. C*, 2014, **XX**, XX

This journal is © The Royal Society of Chemistry 2012

occurrence of condensation reactions between the Si–OH groups and desorption of the H_2O molecules. This is suggestive of the formation of a Si–O–Si network as the framework of the MO film. The cross-linking degree of Si–O–Si network is gradually enhanced with annealing temperature. This is confirmed by the shift of the adsorption peak of the Si–O bonds from 1018 cm^{-1} to 1035 cm^{-1} with increasing annealing temperatures from 220 °C to 500 °C. The absorption peaks associated with the C–H stretching vibrations also become weaker after thermal treatment at 220 °C because of the removal of P123. However, the weak absorption peak at ~2887 cm^{-1} and the peak associated with the Si–C stretching modes at 1270 cm^{-1} are retained at annealing temperatures of up to 500 °C.[22] This observation reflects the good thermal stability of the methylene bridges.
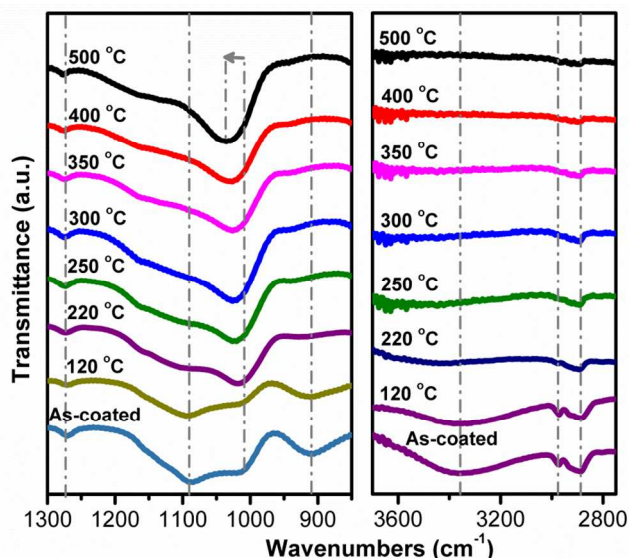

Fig. 1 FTIR spectra of the spin-coated organosilica films as a function of post-annealing temperature. The films were prepared at a P123/BTEE molar ratio of 0.02.
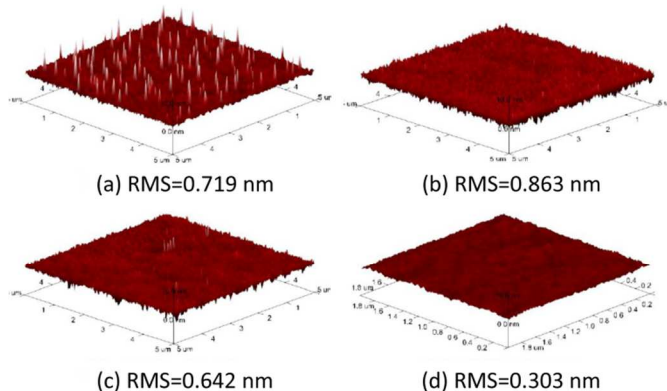

Fig. 2 AFM images of the MO films prepared at a P123/BTEE molar ratio of 0.02: (a) as-prepared; (b) annealed at 350 °C for 1 h; (c) additional annealing at 400 °C for 30 min; and (d) additional annealing at 500 °C for 30 min.

Figure 2 shows the surface morphology of the as-prepared and subsequently annealed films at different temperatures. The as-prepared film features many sharp peaks on its surface; the root-mean-square (RMS) roughness was measured as 0.719 nm, as shown in Fig. 2(a). This is attributed to the aggregation of P123 molecules

located at the film surface. After annealing at 350 °C in N_2 for 1 h, the sharp peaks disappeared and the RMS roughness slightly increased to 0.863 nm, see Fig. 2(b). This is due to the thermal decomposition of P123 in the films, resulting in the formation of microvoids, which can also form near the surface. However, as the annealing temperature is increased to 500 °C, a re-configuration of the amorphous covalent network in the film occurs, resulting in the collapse of the voids and compaction of the films.[24] Therefore, the film surface becomes smoother and exhibits a reduced RMS roughness of 0.303 nm, as shown in Fig. 2(d).
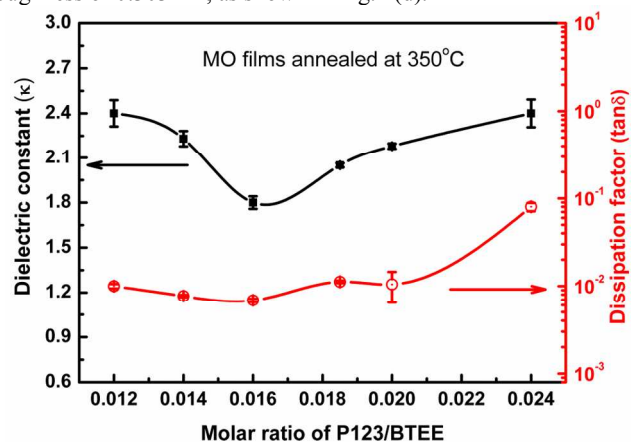

Fig. 3 Dielectric constants (κ) and dissipation factors (tan δ) at 100 kHz of MO films prepared at varying P123/BTEE molar ratios.
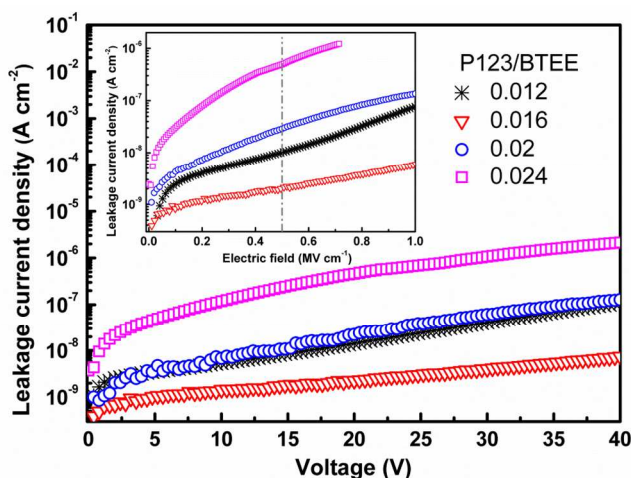

Fig. 4 Dependence of leakage current density on voltage for the MO films prepared at different P123/BTEE molar ratios. The inset shows the leakage current density–electric field profiles of the MO films.

Figure 3 shows the dielectric constant and dissipation factor of the MO films as a function of the P123/BTEE molar ratio. As the P123/BTEE molar ratio increases from 0.012 to 0.016, the measured κ decreases approximately from 2.4 to 1.8. However, when the molar ratio exceeds 0.016, the resulting κ increases at increasing molar ratios of up to 0.024. These observations are explained as follows. As the molar ratio of P123/BTEE (relative concentration of P123) increases, the porosity incorporated in the post-annealed organosilica film rises, leading to the formation of increased free volume with κ = 1 within the film. This causes a decrease in the dielectric constant of the MO film. When the molar ratio is higher than the critical value, the P123 aggregates in the as-prepared films become bigger, while the walls of the organosilica framework become thinner. Therefore, as the decomposition of P123 proceeds

This journal is © The Royal Society of Chemistry 2012

J. Mater. Chem. C, 2014, **XX**, XX | **3**

during annealing at 350 °C, the relatively large generated pores are prone to shrinkage and collapse because of the thin pore walls at high porosities, leading to an increase in the κ value of the MO film.[9] Furthermore, the MO films exhibit small dissipation factors (< 0.015) at P123/BTEE molar ratios of ≤ 0.02. In particular, a P123/BTEE molar ratio of 0.016 generated the lowest κ value, with an associated dissipation factor as low as 0.0068, demonstrating a very small dielectric loss at 100 kHz. Figure 4 shows representative leakage current density–voltage profiles of the prepared MO films. At P123/BTEE molar ratios smaller and larger than 0.016, the resulting MO films demonstrate relatively high leakage current density values that are similar to the trend observed for the dielectric constant. At a P123/BTEE molar ratio of 0.016, the resulting MO film exhibits excellent leakage current characteristics, i.e., its leakage current density is as low as 2.01×10^{-9} A cm^{-2} at 0.5 MV cm^{-1}, as shown in the inset of Fig. 4.
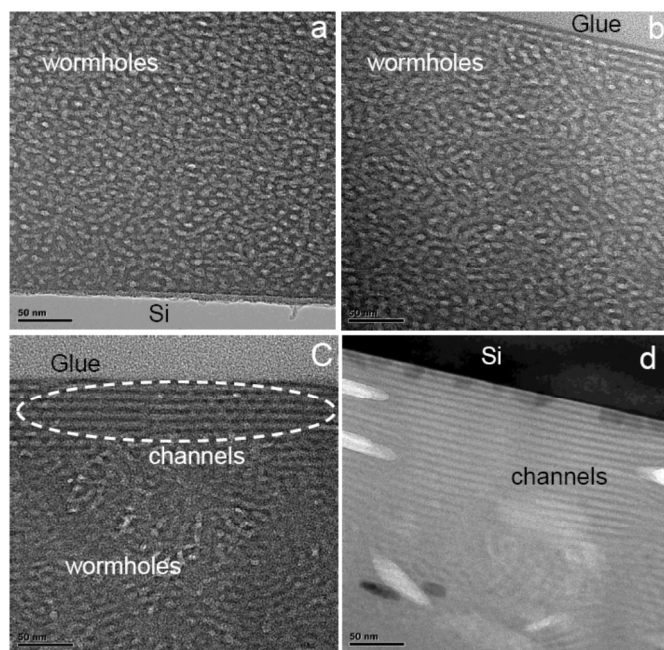

Fig. 5 Cross-section TEM images of the MO films prepared at different P123/ BTEE molar ratios of (a) 0.012, (b) 0.016, (c) 0.02, and (d) 0.024.

The cross-section TEM images of the MO films prepared at different P123/BTEE molar ratios are shown in Fig. 5. MO films prepared at a P123/BTEE molar ratio of 0.012 feature numerous worm-like mesopores arranged in a disorderly fashion that was consistent throughout the film, see Fig. 5(a). As the molar ratio increases to 0.016, the worm-like mesopores become larger. Interestingly, when the molar ratio is increased to 0.02, some well-ordered long mesopores (channel-like arrays) are formed near the film surface, indicating the presence of a mixed phase in the film. By increasing the P123/BTEE molar ratio to 0.024, channel-like arrays with increased order are formed near the substrate interface in addition to the generation of a few large voids, as shown in Fig. 5(d). The observed large voids are ascribed to the development of stress during pyrolysis of the P123 molecules that likely led to the collapse of thinner pore walls. Regardless, the aforementioned phenomena were dependent on the concentration of P123 in the aqueous solution, and can be explained according to Fig. 6. It is well known that when surfactant concentration reaches critical micelle concentration (CMC) for a given system, micelles (thermodynamically stable polymolecular aggregates) start to form

and grow at increasing surfactant (copolymer) concentration.[25,26] Herein, when the P123/BTEE molar ratio is equal to 0.012, the concentration of P123 virtually exceeds its CMC. Thus, P123 micelles form, as indicative of the irregular spheres and short bar-like shapes observed in the TEM images in Fig. 6. As the concentration of P123 increases, the aggregated micelles feature more pronounced worm-like shapes. When the P123 concentration increases to a critical point, the micellar aggregates self-assemble to form channel-like entities, preferentially near the air–MO film and MO film–substrate interfaces, likely because of preferential wetting of the air–film surface and film–substrate interfaces by a specific component, similar to the phenomenon in block copolymer thin films.[27,28] The self-assembled channel-like array domains subsequently become larger with increasing P123 concentration.
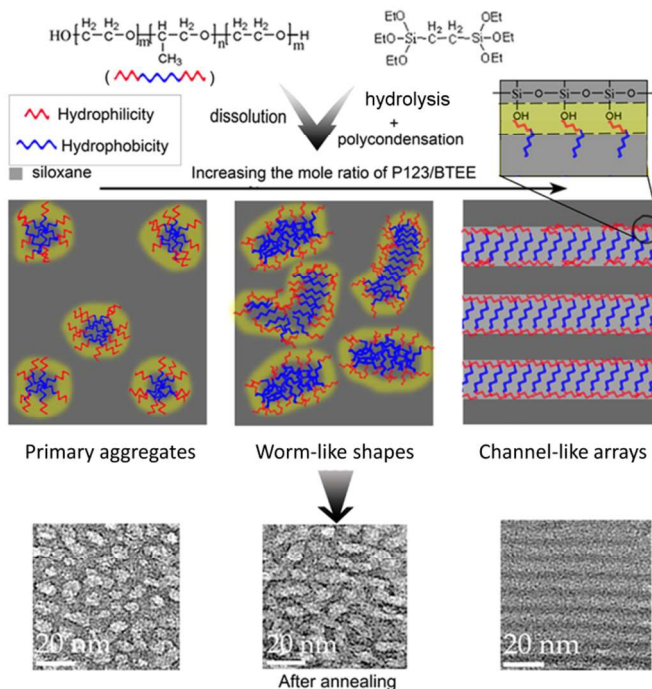

Fig. 6 Schematic diagram of the development of the mesopore structure in the film with increasing P123/BTEE molar ratio.
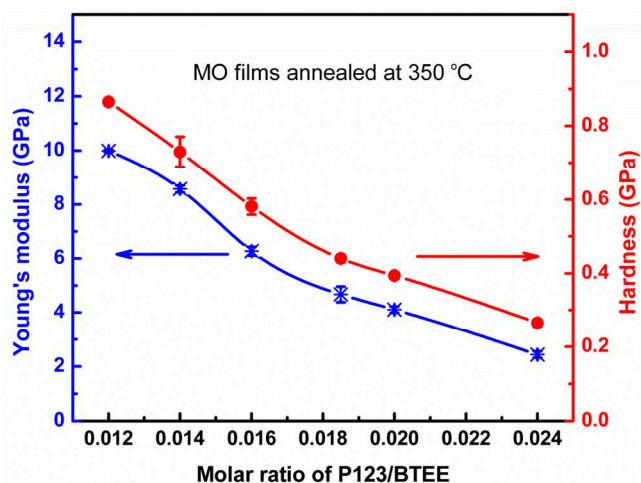

Fig. 7 Young's modulus and hardness of the MO films prepared at different P123/BTEE molar ratios.

4 | *J. Mater. Chem. C*, 2014, **XX**, XX

This journal is © The Royal Society of Chemistry 2012

To evaluate the mechanical properties of the resulting low-κ films, the Young's modulus (E) and hardness (H) were measured, as shown in Fig. 7. Both E and H of the prepared MO films decrease with increasing P123/BTEE molar ratios. As the molar ratio increases from 0.012 to 0.024, E decreases from 10 to 2.44 GPa, and H decreases from 0.865 to 0.265 GPa. This is because a larger P123/BTEE molar ratio results in a higher porosity and thinner pore walls. A P123/BTEE molar ratio of 0.016, which corresponds to the lowest κ value (κ = 1.8) in the present study, generates E and H values of 6.27 GPa and 0.58 GPa, respectively. It has been pointed out that Young's modulus values greater than 4 GPa are adequate for preparing low-κ thin films with a good chemical mechanical polishing stability.[3] Thus, the excellent combination of κ = 1.8 and E = 6.27 GPa would satisfy the dielectric and mechanical requirements for next-generation interlevel dielectrics in the advanced semiconductor industry. However, for practical application purposes, ultralow-κ materials need to possess a hydrophobic character to avoid moisture adsorption. This is because the adsorbed moisture can markedly increase the dielectric constant of the material because the κ value of water is ~80. As a result, the moisture adsorption characteristics of the ultralow-κ material require proper assessment and further engineering of the ultralow-κ material requires attention.

Figure 8(a) compares the dielectric constants of the ultralow-κ film prepared at a P123/BTEE molar ratio of 0.016 before and after the moisture adsorption experiment. Prior to the moisture adsorption experiment, the film displays κ values in the range of 1.80–1.84. After the moisture adsorption experiment at 80% relative humidity (RH) for 12 h, the resulting film displays higher κ values in the range of 2.01–2.07. These data indicate that moisture adsorption leads to an increase of ~12% in the dielectric constant, which is still very low. Moreover, exposure to moisture under the current conditions results in an increased leakage current density of the dielectric, as shown in Fig. 8(b). Under an external electric field of 0.5 MV cm^{-1}, the leakage current density increases from 1.87×10^{-9} to 2.73×10^{-8} A cm^{-2}.

Fig. 9   Comparison of the (a) dielectric constant and (b) leakage current density at room temperature before and after moisture adsorption (80% RH) for the UV-treated ultralow-κ film prepared at a P123/BTEE molar ratio of 0.016.
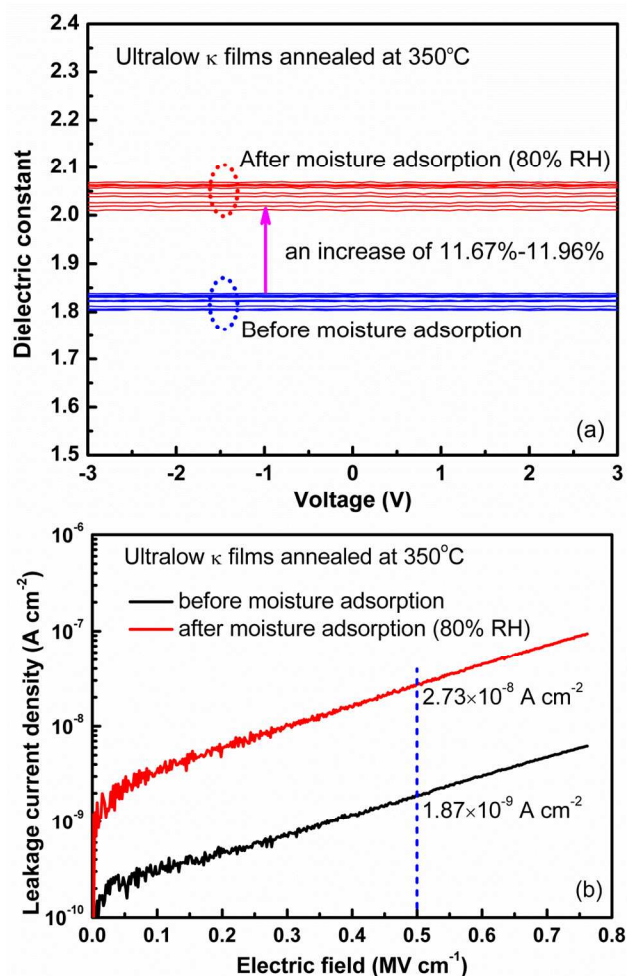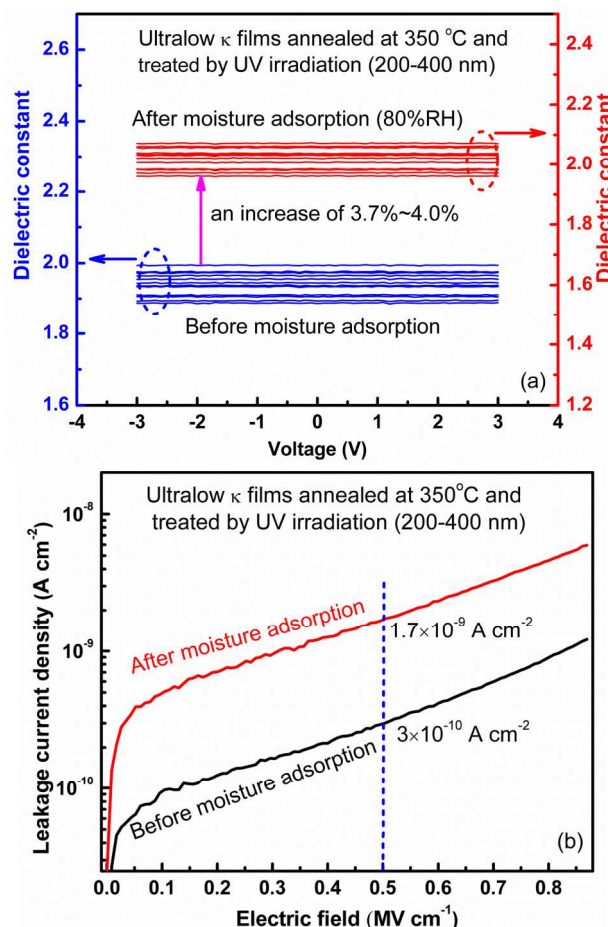

Fig. 8   Comparison of the (a) dielectric constant and (b) leakage current density at room temperature before and after the moisture adsorption experiment (80% RH) for the ultralow-κ film prepared at a P123/BTEE molar ratio of 0.016.

Ultraviolet irradiation techniques have been extensively used to improve the mechanical properties of low-κ materials;[29-31] however, the effect of ultraviolet irradiation on the moisture adsorption characteristics of low-κ materials has not been reported yet. In this study, the ultralow-κ sample was first exposed to ultraviolet irradiation at wavelengths of 200–400 nm for 5 h. The electrical characteristics of the sample were then measured, after which the aforementioned sample was stored in an ambient atmosphere at 80% RH for 15 h. The electrical properties were measured again. Figure 9(a) compares the dielectric constants of the UV-irradiated low-κ films before and after the moisture adsorption experiment. In the

absence of the moisture pre-treatment, the UV-irradiated sample shows κ values ranging from 1.89 to 1.99, which are slightly higher than those of the pristine low-κ film. Following moisture pre-treatment, the κ values of the resulting UV-irradiated films are in the range of 1.96–2.07, corresponding to an increase of ~4%. Comparison of the data with those in Fig. 8 (a) indicates that UV irradiation greatly improves the moisture adsorption resistance of the ultralow-κ material. In addition, UV irradiation can significantly improve the insulating performance of the ultralow-κ material in terms of pre- and post-moisture adsorption, as shown in Fig. 9(b). The resulting leakage current density is as low as 3×10^{-10} A cm^{-2} at 0.5 MV cm^{-1} in the absence of a moisture pre-treatment. Following moisture pre-treatment, the UV-irradiated sample maintains its excellent leakage character, i.e., 1.7×10^{-9} A cm^{-2} at 0.5 MV cm^{-1}. In summary, UV irradiation of ultralow-κ materials not only enhances the moisture adsorption resistance, but also significantly reduces the leakage current density of the material.
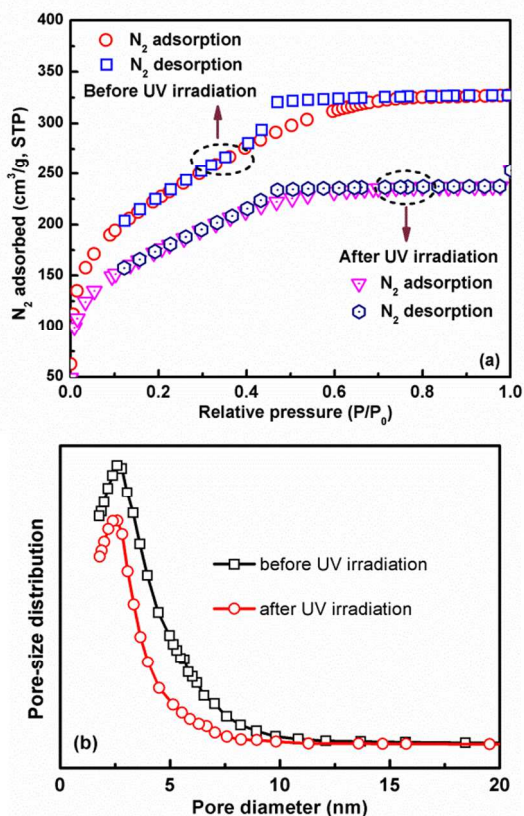

Fig. 10 (a) Nitrogen-sorption isotherms and (b) pore-diameter distribution curves of the ultralow-κ films prepared at a P123/BTEE molar ratio of 0.016 before and after UV irradiation, respectively.

To understand the effect of UV irradiation on the microstructure of the ultralow-κ film, nitrogen physisorption isotherms of the films were measured, as shown in Fig. 10 (a). It can be concluded that after UV irradiation the porosity is decreased, which is indicated by the reduction in the amount of N$_2$ adsorbed. Fig. 10 (b) shows pore-size distributions of the films corresponding to pre- and post-UV irradiation, respectively, single peak is observed at 2.6 nm for both films. Furthermore, it is found that the pore-size distribution becomes narrower after UV irradiation. This indicates that the UV irradiation leads to the formation of more small pores. XPS measurements are used to extract the elemental compositions of the samples. To avoid the influence of adventitious contamination on the sample surface, *in-situ* Ar ion etching is carried out before XPS

measurement. Table 2 shows the atomic percentages and refractive indexes of the films before and after UV-irradiation. It is seen that the UV irradiation decreases the carbon percentage by ~5% and increases the oxygen percentage by ~4%, while the silicon percentage almost keeps constant. In addition, the refractive index of the UV-irradiated film exhibits a slight increase, to some extent, which should relate to a reduction in porosity. It has been reported that the CH$_2$ groups can be removed from the low-κ SiCO:H film during the UV cure.[32] Therefore, we think that during UV irradiation the CH$_2$ groups in the top region of the film are preferentially removed because of enhanced UV irradiation near the surface, meanwhile, the bond breaking-generated free radicals likely react with oxygen in the ambient air. This thus causes a reduction of C percentage and an increase of O percentage in the UV-irradiated film. Following the aforementioned process, rearrangement and densification of the top Si–O–Si network layer occur, which is also demonstrated by the reduction in RMS values, *i.e.*, 0.297 nm for the post-irradiated film versus 0.392 nm for the pre-irradiated film. Regarding the pre-irradiated MO film, H$_2$O molecules can deeply diffuse into the film when it is exposed to moisture, filling up the pores.[33] This definitely causes an increase in the κ value of the MO film. After UV irradiation, the top densification layer, which serves as a sealing layer, can prevent H$_2$O molecules from fast diffusing into the film,[33] thus lowering the increase in κ value after exposure to moisture. In general, hydrophobicity of polymer film reduces as its surface smoothness increases. As shown in Fig. 2, the film surface became smoother and smoother with the post-annealing temperature increasing from 350 to 500 °C. Since the surface RMS roughness varied only within a small range (0.863 ~ 0.303 nm), it is thus inferred that roughness-dependent moisture adsorption on the film surfaces should be similar in a normal low relative-humidity ambient, as revealed by the similar FTIR spectra between 3600 cm^{-1} and 3200 cm^{-1} in Fig. 1. However, owing to the presence of a lot of pores within the MO film, moisture adsorption occurs dominantly within the film rather than the film surface especially in a higher RH (80%) ambient. Therefore, the surface layer character plays a key role in moisture adsorption, as discussed above.

Table 2 Si, C and O atomic percentages and refractive indexes of the films

Sample	Atomic percentage (%)			Refractive index
	Si	C	O	
Before UV irradiation	42.2	18.6	39.2	1.277
After UV irradiation	42.9	14.0	43.1	1.282

During the interconnect fabrication process and IC packaging step, thermal annealing is essential.[34-36] In particular, unlike upper-level interconnects, lower-level interconnects will undergo additional annealing during the fabrication of multilevel interconnects.[37] Therefore, the thermal stability of ultralow-κ materials requires comprehensive evaluation for IC processing; assessing the performance stability at high annealing temperatures is highly desirable. Fig. 11 (a) illustrates the κ values–voltage profiles of the ultralow-κ films prepared at a P123/BTEE molar ratio of 0.016 after annealing at 420 and 500 °C. Thermal annealing at 420 °C further reduces the κ value (i.e., 1.76 ± 0.05) of the film when compared with films annealed at 350 °C. After annealing at 500 °C, the κ value increases to 1.92 ± 0.06 (i.e., < 2.0). Such a small increase in the κ value is likely attributed to a reduction of porosity in the annealed film due to enhanced reconstruction of the Si-O-Si framework at higher temperature, meanwhile, this also indicates that the ultralow-κ material synthesized in our study possesses robust thermal stability. Considering the maximal thermal threshold of 420 °C for the back-end-of-line (BEOL) process, such

6 | *J. Mater. Chem. C*, 2014, **XX**, XX

This journal is © The Royal Society of Chemistry 2012

low κ values at 500 °C can easily satisfy the requirement of bulk dielectric constant for interlevel metal insulator beyond the 10-nm technology node.[2] The leakage current characteristics of the ultralow-κ films annealed at different temperatures are illustrated in Fig. 11 (b). Both films exhibit small leakage current densities in the order of 10^{-9} A cm^{-2} at 0.5 MV cm^{-1}. The mechanical properties of the ultralow-κ films annealed at 420 and 500 °C are listed in Table 3. Compared with previously reported results of merit for low-κ MO films, the currently prepared low-κ films possess superior properties such as ultralow κ values, robust mechanical strength, and excellent leakage current characteristics, even after annealing at 500 °C.
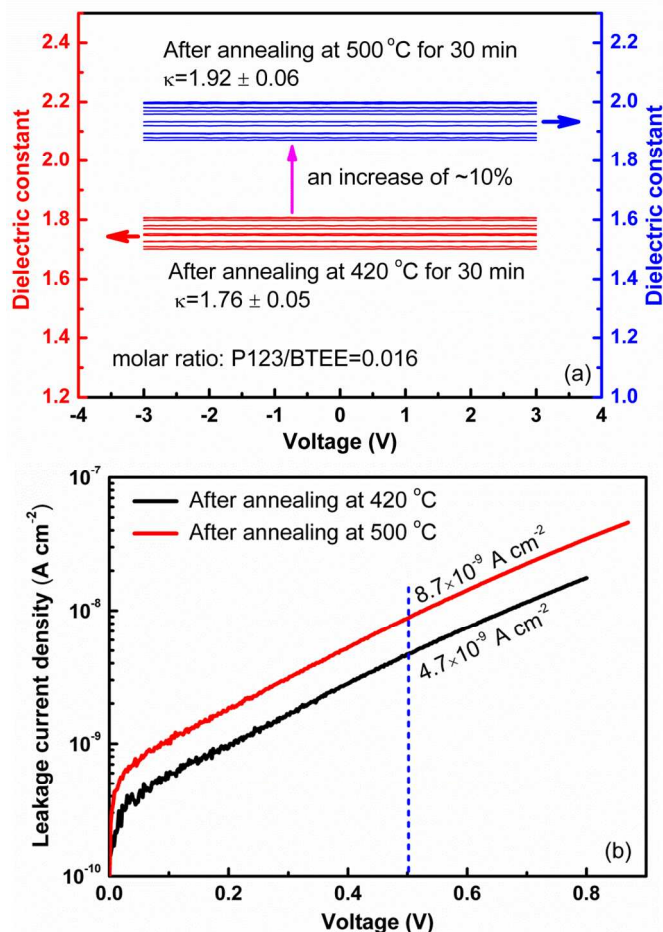

Fig. 11 (a) Dependence of the dielectric constant on voltage at 100 kHz for the films prepared at a P123/BTEE molar ratio of 0.016 after annealing at 420 °C and 500 °C. (b) Leakage current density as a function of voltage for the aforementioned low-κ films.

Conclusions

MO films were prepared using a carbon-bridged precursor 1,2-bis(triethoxysilyl)ethane (BTEE) and a porogen template P123. By optimizing the annealing temperature and P123/BTEE molar ratio, high-performance ultralow-κ MO films were achieved, exhibiting a κ value of 1.80, a small dissipation factor of 0.0068 at 100 kHz, an extremely low leakage current density of 2.01×10^{-9} A cm^{-2} at 0.5 MV cm^{-1}, E of 6.27 GPa, and H of 0.58 GPa. Furthermore, ultraviolet treatment greatly improved the moisture resistance of the MO films, resulting in a substantially smaller increase of 4% in κ following moisture adsorption when compared with an increase of 12% for films that underwent no ultraviolet treatment. In addition, the UV-treated films demonstrated a leakage current density of one order of magnitude lower than that of the untreated films following moisture adsorption. Even after critical high-temperature annealing at 500 °C, the MO films maintained superior performance, as indicated by a κ value of ~1.92, a leakage current density of 7.08×10^{-9} at 0.5 MV cm^{-1}, E of ~9.1 GPa, and H of ~0.8 GPa. Therefore, this type of MO film has great potential as an interlevel insulator in advanced interconnects.

Acknowledgements

[a] State Key Laboratory of ASIC and System, School of Microelectronics, Fudan University, 220 Handan Road, Shanghai 200433, China. E-mail: sjding@fudan.edu.cn; 86-21-55664845

[b] Department of Materials Science, Fudan University, 220 Handan Road, Shanghai 200433, China

Table 3 Comparison of the properties of the current ultralow-κ MO films (prepared at a P123/BTEE molar ratio of 0.016) with other reports.

Ref.	Precursors	Porogen	Dielectric constant (κ)	J (A cm^{-2}) at 0.5 MV cm^{-1}	E (GPa)	H (GPa)	Annealing temperature (°C)
This work	BTEE	P123	1.82 ± 0.02	1.58 × 10^{-9}	6.45 ± 0.15	0.58 ± 0.03	350
			1.76 ± 0.05	3.60 × 10^{-9}	6.75 ± 0.17	0.60 ± 0.02	420
			1.92 ± 0.06	7.08 × 10^{-9}	9.1 ± 0.14	0.8 ± 0.016	500
[23]	BTEE, MTES	P123	2.0 ± 0.05	9 × 10^{-9}	4.05 ± 0.35	0.32 ± 0.03	350
			1.9 ± 0.06	2 × 10^{-7}	6.21 ± 0.3	0.52 ± 0.03	400
			2.0 ± 0.01	2 × 10^{-8}	5.0 ± 0.25	0.56 ± 0.03	500
[38]	BTEE	CTACl	2.9	/	13.3 ± 2.2	0.77 ± 0.06	300
			1.8				400
			1.9				500

This journal is © The Royal Society of Chemistry 2012

J. Mater. Chem. C, 2014, **XX**, XX | **7**

[39]	BTEM	P123	1.85	2.5×10^{-9}	3.8	/	350
[40]	BTEE	Brij-76	2.07	2.0×10^{-8}	5.9	0.6	400
[4]	Tetravinyltetramethylcyclotetrasiloxane (V4D4)	/	3.4	/	3.9	0.5	330
			2.8		/	/	370
			2.1		5.4	0.79	410
[41]	Cyclohexane	Decamethylcyclopentasiloxane	2.05 ± 0.04	/	1 ± 0.1	0.06 ± 0.01	400
			1.85 ± 0.02	1×10^{-8} at 1 MV cm^{-1}	0.59 ± 0.059	0.05 ± 0.007	450
			2.16 ± 0.02	/	2.12 ± 0.168	0.1 ± 0.017	500

References

1   W. W. Lee, P. S. Ho, *MRS Bulletin*, 1997, **10**, 19.
2   ITRS, http://www.itrs.net, *2012*.
3   G. Dubois, W. Volksen, T. Magbitang, R. D. Miller, D. M. Gage and R. H. Dauskardt, *Adv. Mater.*, 2007, **19**, 3989.
4   N. J. Trujillo, Q. Wu, K. K. Gleason, *Adv. Funct. Mater.*, 2010, **20**, 607.
5   M. Seino, W. Wang, J. E. Lofgreen, D. P. Puzzo, T. Manabe and G. A. Ozin, *J. Am. Chem. Soc.*, 2011, **133**, 18082.
6   W. -D. Wang, D. Grozea, A. Kim, D. D. Perovic, and G. A. Ozin, *Adv. Mater.*, 2010, **22**, 99.
7   F. Goethals, I. Ciofi, O. Madia, K. Vanstreels, M. R. Baklanov, C. Detavernier, P. Van Der Voort, and I. Van Driessche, *J. Mater. Chem.*, 2012, **22**, 8281.
8   T. Asefa, M. J. MacLachlan, N. Coombs and G. A. Ozin, *Nature*, 1999, **402**, 867.
9   A. R. Balkenende, F. K. de Theije and J. C. K. Kriege, *Adv. Mater.*, 2003, **15**, 139.
10 D. Y. Zhao, P. D. Yang, N. Melosh, J. L. Feng, B. F. Chmelka, G. D. Stucky, *Adv. Mater.*, 1998, **10**, 1380.
11 H. Yang, N. Coombs, I. Sokolov, G. A. Ozin, *Nature*, 1996, **381**, 589.
12 H. W. Hillhouse, T. Okubo, J. W. van Egmond, M. Tsapatsis, *Chem. Mater.*, 1997, **9**, 1505.
13 R. A. Pai, R. Humayun, M. T. Schulberg, A. Sengupta, J. N. Sun and J. J. Watkins, *Science*, 2004, **303**, 507.
14 R. A. Pai, J. J. Watkins, *Adv. Mater.*, 2006, **18**, 241.
15 J. M. Park, J. K. Choi, C. J. An, M. L. Jin, S. Kang, J. Yun, B.S. Kong, and H. T. Jung, *J. Mater. Chem. C.*, 2013, **1**, 3414.
16 S. M. Gates, D. A. Neumayer, M. H. Sherwood, A. Grill, X. Wang, M. Sankarapandian, *J. Appl. Phys.*, 2007, **101**, 1342.
17 Y. Lin, T. Y. Tsui, J. J. Vlassak, *J. Electrochem. Soc.*, 2006, **153**, F144.
18 B. D. Hatton, K. Landsdron, W. J. Hunks, *Mater. Today*, 2006, **9**, 24.
19 W. E. Tenhaeff, K. K. Gleason, *Adv. Funct. Mater.*, 2008, **18**, 979.
20 K. Maex, M.R. Baklanov, and D. Shamiryan, *J. Appl. Phys.*, 2003, **93**, 8800.
21 L. Jia, C. Guo, L. Yang, J. Xiang, Y. Tang, C. Liu, H. Liu, *J. Colloid Interface Sci.*, 2010, **345**, 332.
22 Y. Liang, R. Anwander, *Microporous Mesoporous. Mater.*, 2004, **72**, 153.
23 S. Fu, K. -J. Qian, S. -J. Ding, D. W. Zhang, *J. Electron. Mater.*, 2011, **40**, 2139.
24 E. Rusli, M. R. Wang, T. K. S. Wong, M. B. Yu, C. Y. Li, *Diamond Relat. Mater.* 2006, **15**, 133.
25 L. Nicole, C. Boissière, D. Grosso, A. Quach and C. Sanchez, *J. Mater. Chem.*, 2005, **15**, 3598.
26 P. Alexandridis, T. A. Hatton, *Colloids Surf, A*, 1995, **96**, 1.
27 L. Song, D. Feng, N. J. Fredin, K. G. Yager, R. L. Jones, Q. Wu, D. Y. Zhao, B. D. Vogt, *ACS Nano*, 2010, **4**, 189.
28 R. A. Segalman, *Mater. Sci. Eng, R.*, 2005, **48**, 191.
29 F. Iacopi, Y. Travaly, B. Eyckens, C. Waldfried, T. Abell, E. P. Guyer, D. M. Gage, R. H. Dauskardt, T. Sajavaara, K. Houthoofd, P. Grobet, P. Jacobs, K. Maex, *J. Appl. Phys.* 2006, **99**, 053511.
30 S. Godavarthi, Q.T. Le, P. Verdonck, S. Mardani, K. Vanstreels, E. Van Besien, M.R. Baklanov, *Microelectron. Eng.*, 2013, **107**, 134.

31 C. Y. Kim, R. Navamathavan, H. S. Lee, J.-K. Woo, M. T. Hyun, K.-M. Lee, W. Y. Jeung, C. K. Choi, *Thin Solid Films*, 2011, **519**, 6732.
32 P. Verdonck, D. D. Roest, S. Kaneko, R. Caluwaerts, N. Tsuji, K. Matsushita, N. Kemeling, Y. Travaly, H. Sprey, M. Schaekers, G. Beyer, Surf. Coat. Technol., 2007, **201**, 9264
33 F. Goethals, M. R. Baklanov, I. Ciofi, C. Detavernier, P. Van Der Voort, I. Van Driessche, Chem. Commun., 2012, **48**, 2797
34 C. K. Choi, C. Y. Kim, R. Navamathavan, H. S. Lee, J. K.Woo, M. T. Hyun, H. J. Lee, W. Y. Jeung, *Curr. Appl. Phys.*, 2011, **5**, S109.
35 A. M. Urbanowicz, K. Vanstreels, P. Verdonck, E. V. Besien, T. Christos, D. Shamiryan, S. De Gendt, M. R. Baklanov, *J. Vac. Sci. Technol. B*, 2011, **29**, 032201.
36 E. Hong, S. Demuynck, Q. T. Le, M. Baklanov, L. Carbonell, M.V. Hove, M. Meynen, *Microelectron. Eng.*, 2007, **84**, 2582.
37 Y.-M. Chang, W.-Y. Chang, J.-F. Huang, J. Leu, Y.-L. Cheng, *Thin Solid Films*, 2013, **528**, 67.
38 B. D. Hatton, K. Landskron, W. Whitnall, D. D. Perovic and G. A. Ozin, *Adv. Funct. Mater.*, 2005, **15**, 823.
39 J. S. Rathore, L. V. Interrante, G. Dubois, *Adv. Funct. Mater.*, 2008, **18**, 4022
40 F. Goethals, E. Levrau, G. Pollefeyt, M. R. Bakanov, I. Ciofi, K. Vanstreels, C. Detavernier, I. Van Driessche and P. Van Der. Voort, *J. Mater. Chem. C*, 2013, **1**, 3961.
41 L. Sungwoo, Y. Jaeyoung, Y. Sanghak, L. Jaewon, J. Donggeun, J. –H. Boo, K. Hyoungsub and C. Heeyeop, *Jap. J. Appl. Phys.*, 2007, **46**, 536.

8 | *J. Mater. Chem. C*, 2014, **XX**, XX

This journal is © The Royal Society of Chemistry 2012